Future Projection of Extreme Heavy Snowfall Events With a 5-km Large Ensemble Regional Climate Simulation

doi: 10.1029/2019JD030781

JGR Atmospheres

RESEARCH ARTICLE
10.1029/2019JD030781

Future Projection of Extreme Heavy Snowfall Events With a 5-km Large Ensemble Regional Climate Simulation

T. Sasai[1], H. Kawase[2], Y. Kanno[3], J. Yamaguchi[1], S. Sugimoto[4], T. Yamazaki[1], H. Sasaki[2], M. Fujita[4], and T. Iwasaki[1]

[1]Graduate School of Science, Tohoku University, Sendai, Japan, [2]Meteorological Research Institute, Japan Meteorological Agency, Tsukuba, Japan, [3]Institute for Space–Earth Environmental Research, Nagoya University, Nagoya, Japan, [4]Japan Agency for Marine-Earth Science and Technology, Yokohama, Japan

Key Points:
- We examined a mechanism for extreme snowfall events with a new ensemble data set for Japan
- Large-scale ensemble 5-km grid simulations were conducted with a regional climate model
- Future cold air outbreaks increase extreme snowfall events over the mountains of Japan on the side of the Sea of Japan

Supporting Information:
- Supporting Information S1

Correspondence to:
T. Sasai,
taka.s.h.g@gmail.com

Citation:
Sasai, T., Kawase, H., Kanno, Y., Yamaguchi, J., Sugimoto, S., Yamazaki, T., et al. (2019). Future projection of extreme heavy snowfall events with a 5-km large ensemble regional climate simulation. *Journal of Geophysical Research: Atmospheres*, *124*, 13,975–13,990. https://doi.org/10.1029/2019JD030781

Received 8 APR 2019
Accepted 26 NOV 2019
Accepted article online 16 DEC 2019
Published online 28 DEC 2019

Abstract We have recently experienced several heavy snowfall events, but still do not sufficiently understand how global warming will impact changes in local extreme snowfall events. The analysis relevant to the extreme events requires ensemble experiments with high-resolution regional climate modeling. In this study, we use a large number of ensemble warming projections downscaled dynamically to 5-km grids to examine the differences in distribution and mechanism in extreme snowfall events over Japan between present and future climates. Japan has two typical snowfall patterns, the winter monsoon and the south coast cyclone patterns. The domain-averaged amount of extreme snowfall in the south coast cyclone pattern regions appear to decrease with the rise in temperatures. Meanwhile, the winter monsoon pattern regions showed little change as the increases in extreme snowfall in the mountainous areas are canceled out by the decrease in the coastal areas. Based on the existing mechanism of normal snowfall, the increase in mountain snow is caused by a temporary intensification of cold air outbreaks. The amount of the cold air blowing from Japan Sea clearly increases only during the days preceding the extreme snowfall event, and as the cold dry air obtains more latent heat over the ocean, the precipitable water vapor increases. The winter monsoon then transports this air over land where the intensification of precipitation results from orographic updraft. This sequence of processes beginning with cold air outbreaks may have a stronger control over extreme snowfall phenomena on the warmer field.

1. Introduction

Two general pressure systems are associated with snowfall: a "lake or ocean effect snow pattern" (e.g., as found downwind of the Great Lakes, in the Norwegian Sea, and in the Sea of Japan) and a "snowstorm pattern" caused by extratropical cyclones (e.g., those developing over the eastern coast of North America and Pacific side Japan). In Japan, the ocean effect and snowstorm patterns correspond to "winter monsoon" and "south coast cyclone" patterns, respectively (Figure S1 in the supporting information). Many studies have investigated several processes related to normal snowfall, and Magono (1966) showed that the winter monsoon pattern is caused by cold air outbreaks from polar regions to Japan islands as the mechanism for normal snowfall. Recent studies have noted distinct regional characteristics of snowfall during heavy snowfall events caused by the two pressure patterns (Kawase et al., 2018). Moreover, heavy snowfall is increasing in frequency and amount in some mountainous regions as the climate warms (Kawase et al., 2016), but is decreasing on average in regions where less precipitation falls as snow (de Vries et al., 2014; Lute et al., 2015).

The IPCC AR5 (2014) states that regional meteorological extreme events have been gradually increasing because of global warming. However, as noted in the IPCC AR5 (2013) and O'Gorman (2014), it is difficult to quantitatively estimate the change in snowfall caused by warming. An extreme snowfall event is a mesoscale meteorological phenomenon that can pose a threat to life and/or property, thus severely impacting human life. Heavy snowfall has a large effect on the total annual snowfall amount (Guan et al., 2013; Lute & Abatzoglou, 2014), suggesting that it also plays a vital role in water resource availability. The regional-scale impact of warming on snow distributions simulated using regional climate models (RCM) has been investigated by several studies (e.g., de Vries et al., 2014; Frei et al., 2018; Kawase et al., 2016; Lute et al., 2015). By examining the effects of warming on representative snowfall mechanisms using the

meteorological output from various RCM experiments, we can comprehensively understand the relationship between snowfall and global warming.

As extreme snowfall is rare and probabilistic in nature and is affected more by internal variability (e.g., temporal changes in the prevailing westerlies and Arctic Oscillation) than by external perturbation (e.g., temperature rise), extracting temporal trends in incidental extreme snowfall events from a single or even multiple simulations is difficult. Therefore, the climatic relationship between extreme snowfall and warming shift is evaluated using uncertainties derived from ensemble experiments of RCM simulations. Recently, a large number of RCM ensemble climate projections has become available because of continuous advancements in computational capacity. The availability of these ensembles provides an opportunity to improve our understanding of the uncertainty of long-term projections, and even to investigate extreme meteorological events with probability density function (PDF) and/or event attribution approaches (e.g., Carril et al., 2012; Christidis et al., 2013; Inatsu et al., 2015; Khaliq et al., 2014; Mizuta et al., 2017). A large number of ensemble members provides a smoothly shaped PDF useful for extracting the probability of extreme events. The difference in PDFs from present and future (warmer) conditions can be used to determine the uncertainty of projections of future extreme snowfall events.

Most ensemble experiments have been conducted at coarse spatial resolution (>100 km) and with climate change projections from AOGCM (Collins et al., 2013). A few studies have used large-scale ensemble experiments with several tens of kilometer resolution (e.g., Inatsu et al., 2015; Mizuta et al., 2017; Sugimoto et al., 2018), but most large-scale ensemble data sets have resolutions that are too coarse to assess mesoscale extreme snowfall events (e.g., Fowler et al., 2007; Mizuta et al., 2017). To accurately simulate mesoscale meteorological phenomena, several studies have indicated the need to include the effects of regionality along with complicated topography (Ishizaki et al., 2012; Kawase et al., 2015, 2016; Sugimoto et al., 2018), requiring higher-resolution simulations.

Projections of how rare, extreme snowfall events will be impacted by the warming shift include large uncertainties because of the limited number of simulations available from high-resolution ensemble experiments. (e.g., Collins et al., 2013; Deser et al., 2012; Xie et al., 2015). Inatsu et al. (2015), in an ensemble experiment combining three RCMs and three GCMs over northern Japan, demonstrated that the uncertainty of meteorological parameters largely depends on the lateral boundary conditions. The "Database for Policy Decision-Making for Future Climate Change" (d4PDF), a state-of-the-art, large-scale, high-resolution ensemble data set of climate projections, has made available a 20-km resolution data set for the East Asia region (Fujita et al., 2018; Mizuta et al., 2017; Murata et al., 2013; Sasaki et al., 2011). However, to more accurately understand extreme snowfall as a mesoscale event, large-scale ensemble experiments using high spatial resolution are required.

In this study, we analyze the change in extreme snowfall events caused by projected future warming, and examine their relationship with cold air outbreaks as a mechanism for extreme snowfall. To detect pure warming-related effects (excluding internal variability), we conducted a large number of ensemble experiments at 5-km resolution dynamically downscaled from the 20-km resolution RCM of the d4PDF data set. Japan has many of the world's snowiest cities. These cities are affected by the two pressure patterns favorable for snowfall that cause snowfall in topographically complex regions. Thus, we simulate snow events over central Japan and analyze these events using a general extreme value (GEV) distribution. In addition, we examine the difference between present and future snowfall for each general snowfall pattern to identify the mechanisms involved in extreme snowfall events, including their relationship with cold air outbreaks. We extracted >1,000 years of data from the regional d4PDF data set, and conducted climate simulations using three warming scenarios.

2. Data and Methods

2.1. Data

To obtain probabilistic future projections of low-frequency localized snowfall events, the d4PDF regional climate data set that has scenarios of 2 K and 4 K warmer climates than the preindustrial climate is used. The original d4PDF data set consists of outputs from global simulations using MRI-AGCM3.2 (JMA, 2007) and outputs from regional downscaling simulations covering the area of Japan using the Non-Hydrostatic

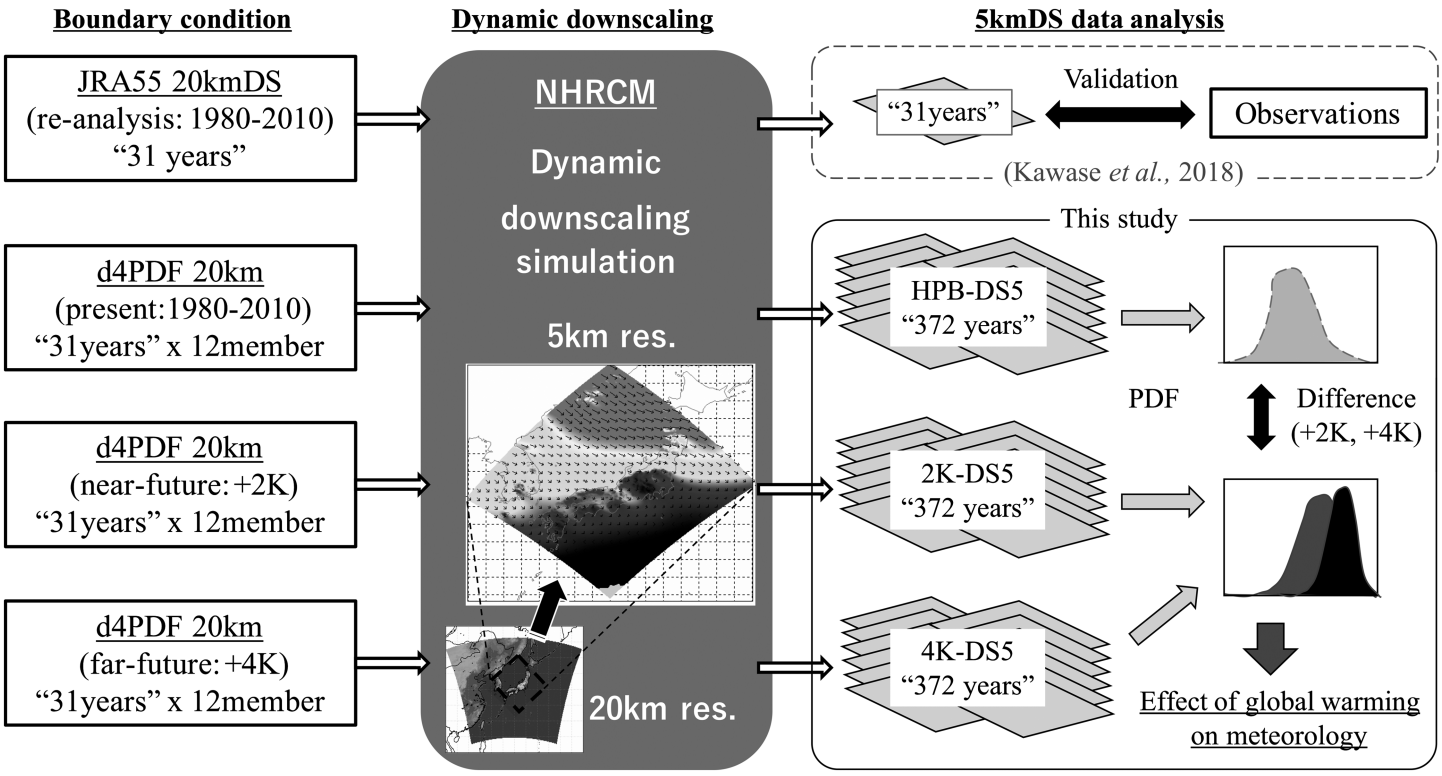

Figure 1. Design of ensemble warming projection using a regional climate model.

Table 1
Model Settings

	5-km DS
Model	Non-Hydrostatic Regional Climate Model (NHRCM)
Governing equations for atmospheric motions	Fully compressible nonhydrostatic equations
Horizontal discretization	Grid point method
Advection term	4th-order scheme with advection correction
Map projection	Lambert Conformal Conic Projection
Vertical coordinate systems	Z*-coordinate
Vertical grid resolution	40 m (surface layer), 904 m (top layer)
Top level of atmosphere	21,801 m (about 40 hPa)
Coarse line	GLCC
Initial time	24 July
Forecast time	24 July to 30 August of the next year
Integrated-time Step	20 s
Lateral boundary value	d4PDF data set from 20-km NHRCM
Lateral boundary relaxation	Enable
Lateral boundary of relaxation zone	50 km (10 pixels)
Adaptive moisture diffusion	3 m/s (vertical velocity threshold)
Calculated-time step for radiation process	15 min
Land surface type	Vegetation, urban, ocean, cloud, and sea ice
Land surface flux	Improved SiB and urban canopy model

Regional Climate Model (NHRCM; Sasaki et al., 2011; Murata et al., 2013) with horizontal grid spacings of 60 and 20 km, respectively. External forcing in the regional downscaling simulations was derived from MRI-AGCM3.2 simulations as the parent model (e.g., greenhouse gases, atmospheric ozone, and aerosols). Boundary conditions, except for sea surface temperature (SST), were derived from the spatial and temporal variations of MRI-CCM (Deushi & Shibata, 2011) and MRI-CGCM3 (Yukimoto et al., 2012). The climate of the latter half of the twentieth century is simulated for 6,000 years (3,000 years for the area of Japan), and 2-K and 4-K warmer climates are simulated for 3,240 and 5,400 years, respectively (http://www.miroc-gcm.jp/~pub/d4PDF/index_en.html). Differences among these three simulations are caused by variations of the external forcing and SST (including sea ice concentration), which have the 50, 90, and 54 perturbative patterns in the present, and the 2-K and 4-K warmer climates, respectively (Mizuta et al., 2017). For the 2-K and 4-K scenarios, SST, which is the difference between the present and future climates, was set using the future SST distribution projected by six CMIP5 models (Table 2 in Mizuta et al., 2017). The fundamental boundary conditions and the perturbative pattern of the present scenario were derived from the spatial and temporal variations of COBE-SST2 (Hirahara et al., 2014).

2.2. Ensemble Design

Dynamical downscaling to 5-km horizontal resolution was performed for NHRCM simulations from the d4PDF 20-km resolution regional climate data set (Figure 1 and Table 1; Mizuta et al., 2017). The NHRCM simulations employed: a three-ice bulk cloud microphysics scheme including an ice crystal falling process (Ikawa et al., 1991); the Kain-Fritsch convection

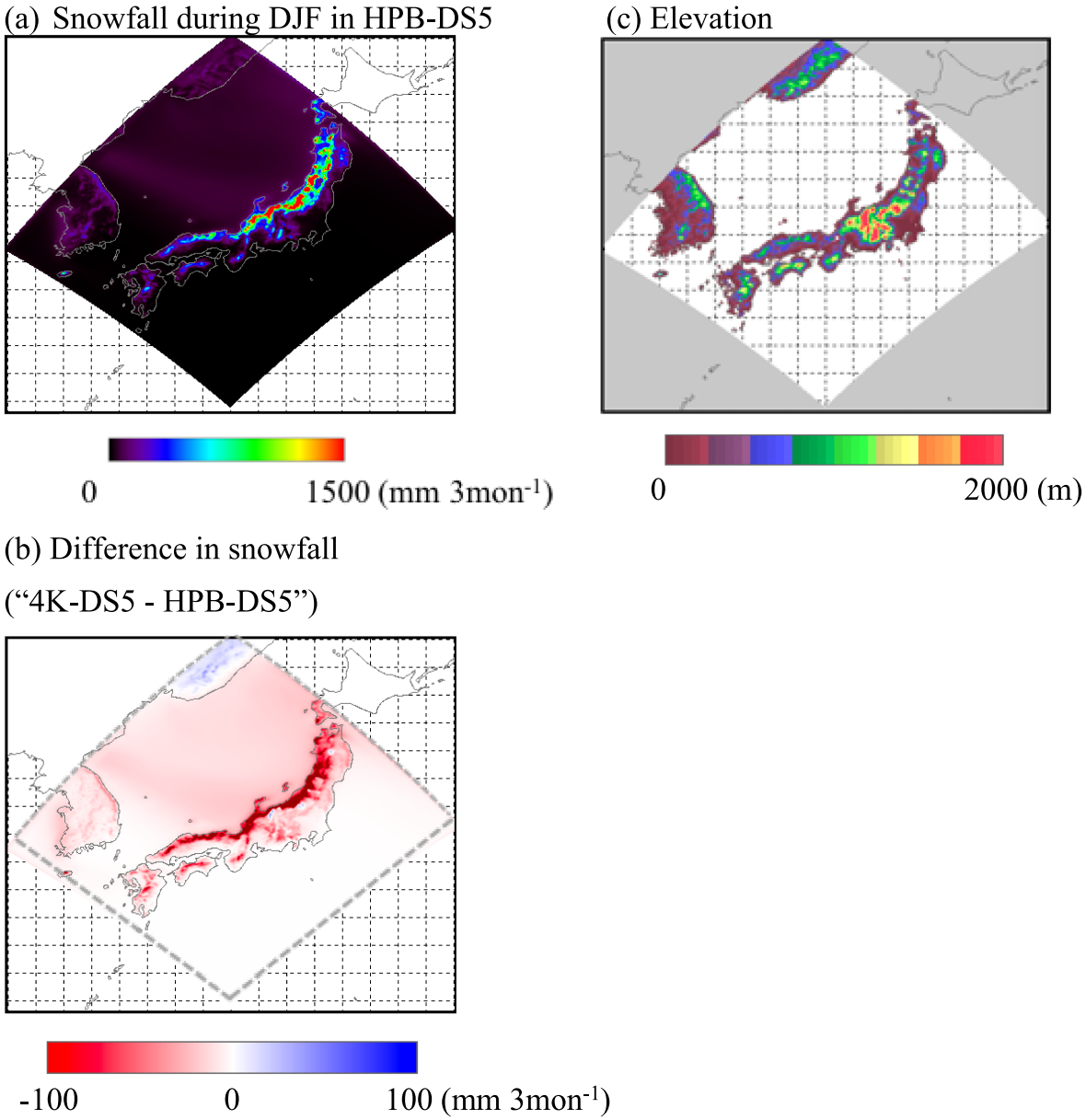

Figure 2. Spatial distributions of average winter (DJF) snowfall for (a) HPB-DS5, (b) the difference between HPB- and 4 K-DS5, and (c) elevation. Snowfall is calculated as a climatology for HPB- and 4 K-DS5.

scheme (Kain & Fritsch, 1993); the Mellor-Yamada-Nakanishi-Niino Level 3 turbulence kinetic energy scheme for planetary boundary layer conditions (Nakanishi & Niino, 2004); the Kitagawa (2000) approach for cloud radiative effects; a clear-sky radiation scheme (Yabu et al., 2005); the cover partial condensation scheme for radiation process to cloud (Sommeria & Deardorff, 1977); the SiB land surface model (Sellers et al., 1986) with improvements by Sato et al. (1989) and Hirai et al. (2007); and the urban canopy and snow model (Aoyagi & Seino, 2011; Ito et al., 2018). The spin-up period is 24–31 July, and the subsequent 1-year period (1–30 August of the following year) is used as the analysis period. The horizontal grid (321 × 301) covers central Japan (26.00–46.05°N, 123.50–147.55°E), and the number of atmospheric vertical level is 50. topographic data from GTOPO-30 were preprocessed using the envelope detection approach.

Model settings used here were chosen based on previous work (Kawase et al., 2018; Sugimoto et al., 2018), and were used to execute a large number of ensemble experiments in which the only inputs that change are the lateral boundary conditions. The present scenario assumes a climatic field averaged over 1980–

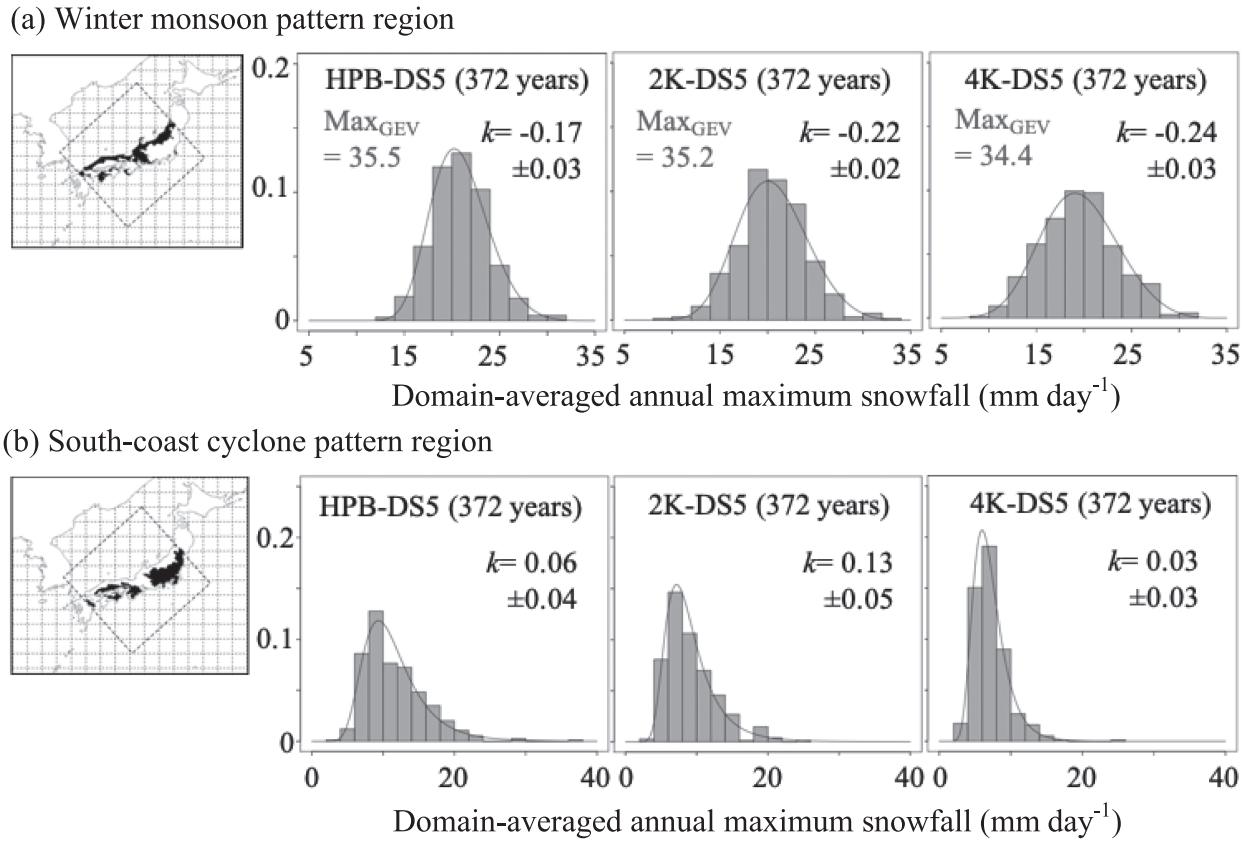

Figure 3. Statistical comparison of extreme snowfall between (a) the winter monsoon and (b) south coast cyclone pattern regions among HPB-, 2K-, and 4K-DS5. The region is shown in Figure 11 of Kawase et al. (2018). Max_{GEV} is the maximum snowfall value statistically defined by the GEV distribution (SLSC < 0.03) and k is the shape parameter of the GEV distribution with error range $\pm\sigma$.

2010 (HPB-DS5), and the near- and far-future scenarios assume climatic fields in which the global mean air temperature has increased by 2 K or 4 K from the preindustrial period, based on CMIP5 results for the middle and end of the 21st century (2K-DS5 and 4K-DS5, respectively). Each member of the future scenario covers a 31-year period. Individual member scenarios from HPB-DS5 were randomly extracted from the full d4PDF, and each member scenario from 2K-DS5 and 4K-DS5 was extracted from the six SST patterns of the CMIP5 models (2 × 6 SST patterns = 12 members; Mizuta et al., 2017). Thus, NHRCM was executed for a total of 1,116 years (= 31 years × 12 members × 3 scenarios). The model settings used were validated using the Japanese 55-year reanalysis data set (JRA55; Kobayashi et al., 2015). Evaluation results are in reasonable agreement with observations (Kawase et al., 2018; Sugimoto et al., 2018).

2.3. Methods

To evaluate the frequency of occurrence of rare snowfall events using a PDF, we first compensate for the deficiency in values within the extreme range using the GEV distribution of the extreme value theory. Although our computational resources allowed us to conduct a model experiment for a total of 1,116 climate years (= 372 years × 3 scenarios), the resulting number of samples is still insufficient to statistically express the parent population. Thus, extreme snowfall events are evaluated using a GEV distribution [F(x)] that includes the standard least squares criterion (SLSC; Coles, 2001; Fujibe, 2011):

$$F(x) = exp\left[-\{1.0-k(x-b)/a\}^{1/k}\right], \quad (1)$$

where a and b are the scale and location parameters, respectively. Based on the shape parameter of GEV (k), we determine whether the distribution is Fréchet ($k < 0$) or Weibull ($k > 0$). Fréchet (Weibull) distributions have finite lower (upper) and infinite upper (lower) endpoints. A statistical rare event is defined as the day

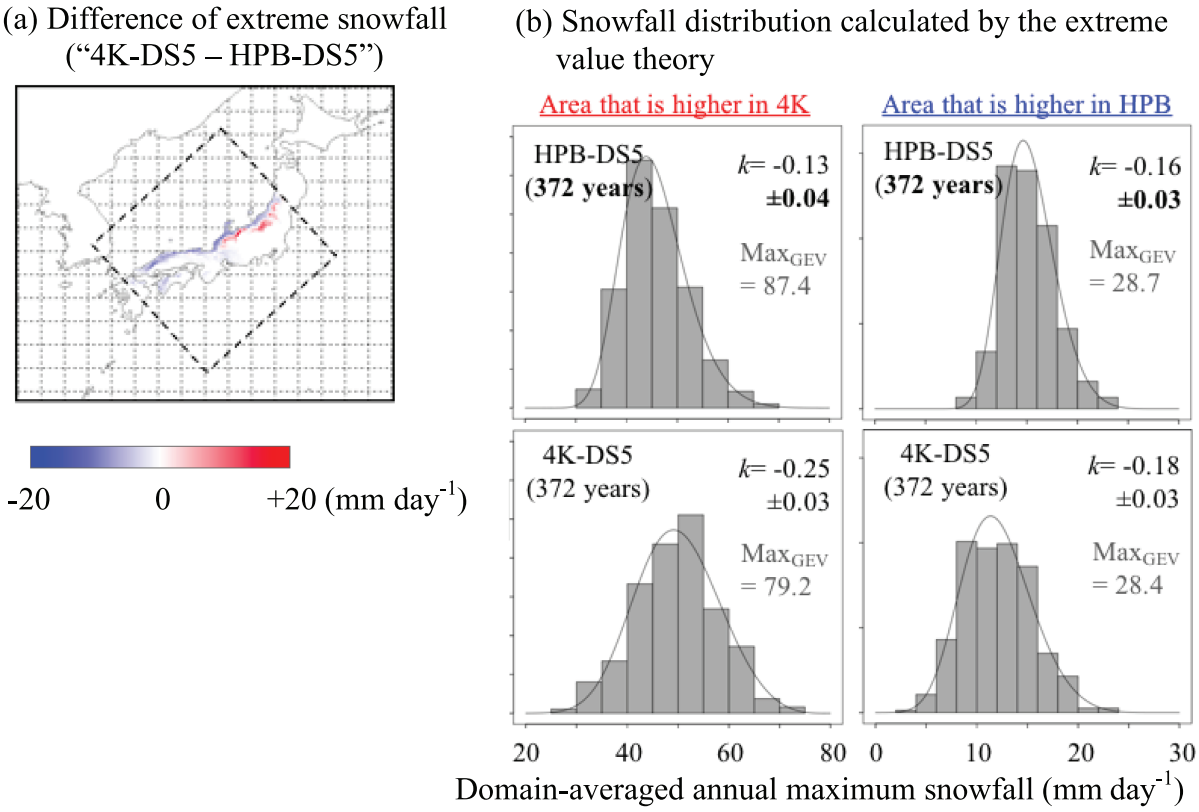

Figure 4. (a) Difference in extreme snowfall between HPB- and 4 K-DS5 in the winter monsoon pattern region. (b) Comparison of extreme snowfall distributions between increasing (red area [a]) and decreasing (blue area) regions.

that has the highest daily value for a property of interest in a 1-year period. Thus, we extract 372 extreme event samples from three experiments. The SLSC value can be used to determine if the sample size is statistically sufficient for the analysis (SLSC < 0.03).

We estimated spatial and temporal variations in cold air mass flux using the isentropic cold-air analysis tool, which defines the mass below a threshold potential temperature as a cold air mass (Iwasaki et al., 2014; Kanno et al., 2016; Shoji et al., 2014). The cold air mass is calculated as a difference of atmospheric pressure between geographical and isentropic surfaces:

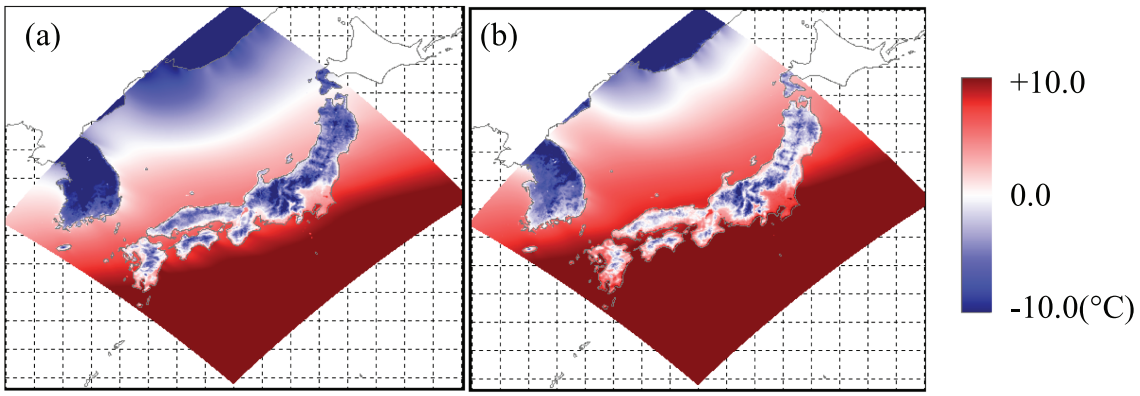

Figure 5. Spatial variations of air temperature (2 m above the surface) on an extreme snowfall day in the winter monsoon pattern region for (a) HPB-DS5 and (b) 4K-DS5.

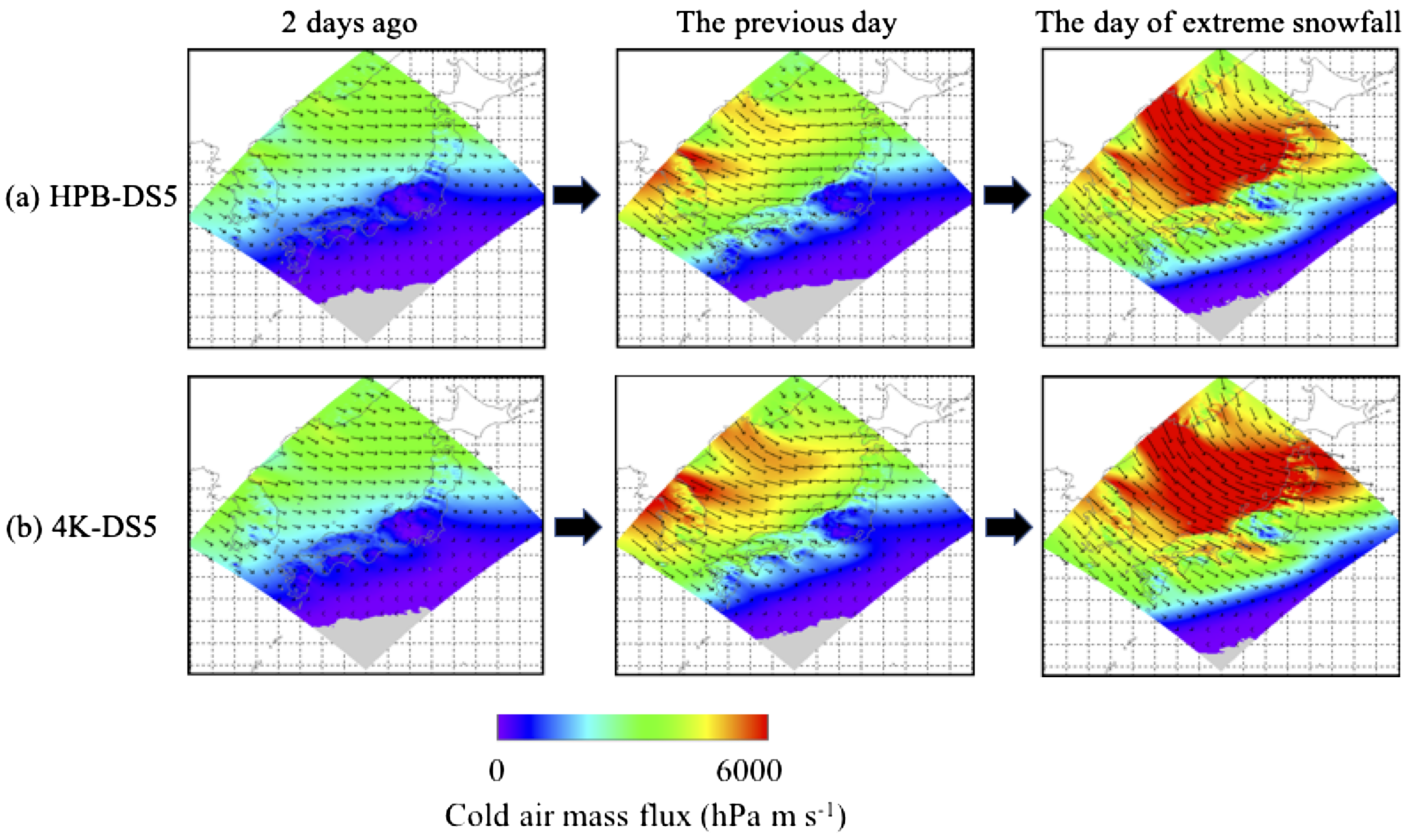

Figure 6. Spatial variations of cold air mass flux derived from a temporal composite analysis of 3 days before an extreme snowfall event for (a) HPB-DS5 and (b) 4K-DS5. The cold air mass flux was calculated from the three-dimensional potential temperature using the approach of Iwasaki et al. (2014). All panels are a temporal composite of the 372 extreme snowfall days during a 372-year period. Gray areas indicate that the cold air mass flux is zero.

$$DP \equiv \rho_s - \rho(\theta_T), \tag{2}$$

where ρ_s is the surface pressure and $\rho\,(\theta_T)$ is the pressure on the isentrope $\theta = \theta_T$. Cold air mass thickness is defined as the potential temperature below θ_T when the hydrostatic equilibrium condition is satisfied and when no static unstable layer exists. Using the mass stream function (climate mean position of equatorward flow) diagnosed by the mass-weighted isentropic zonal mean (Iwasaki et al., 2014), the threshold potential temperature of cold air was set as 280 K in HPB-DS5 (i.e., $\theta_T = 280$ K). Previous studies explore historical and future changes in cold air mass flux (e.g., Kanno et al., 2016), and suggested that, by changing the thermodynamic equilibrium point due to global warming, the boundary layer height between warm air blowing from lower latitudes and cold polar air is essentially moved. Thus, we changed the threshold potential temperature for the future scenarios. The difference of domain-averaged potential temperature at 850 hPa in HPB-DS5 from 280 K is added to the original threshold value of 280 K (i.e., $\theta_T = 281.9$ K for 2K-DS5 and 284.3 K for 4K-DS5). The cold air mass flux is integrated from ρ_s to $\rho\,(\theta_T)$ as follows:

$$\boldsymbol{F} \equiv \int_{\rho_{(\theta T)}}^{\rho_s} \boldsymbol{v}\, d\rho, \tag{3}$$

where $\boldsymbol{v}$ is the horizontal wind.

3. Results

We examined the spatial distribution in snowfall accumulated during winter (December-January-February) and its future change using all the ensemble experiments. The ensemble mean spatially shows a typical winter monsoon pattern (average snowfall = 64.8 mm 3 month^{-1}). Much greater snowfall is found near the Sea of Japan than near the Pacific (Figures 2a and 2b), and higher elevations experience heavier snowfall

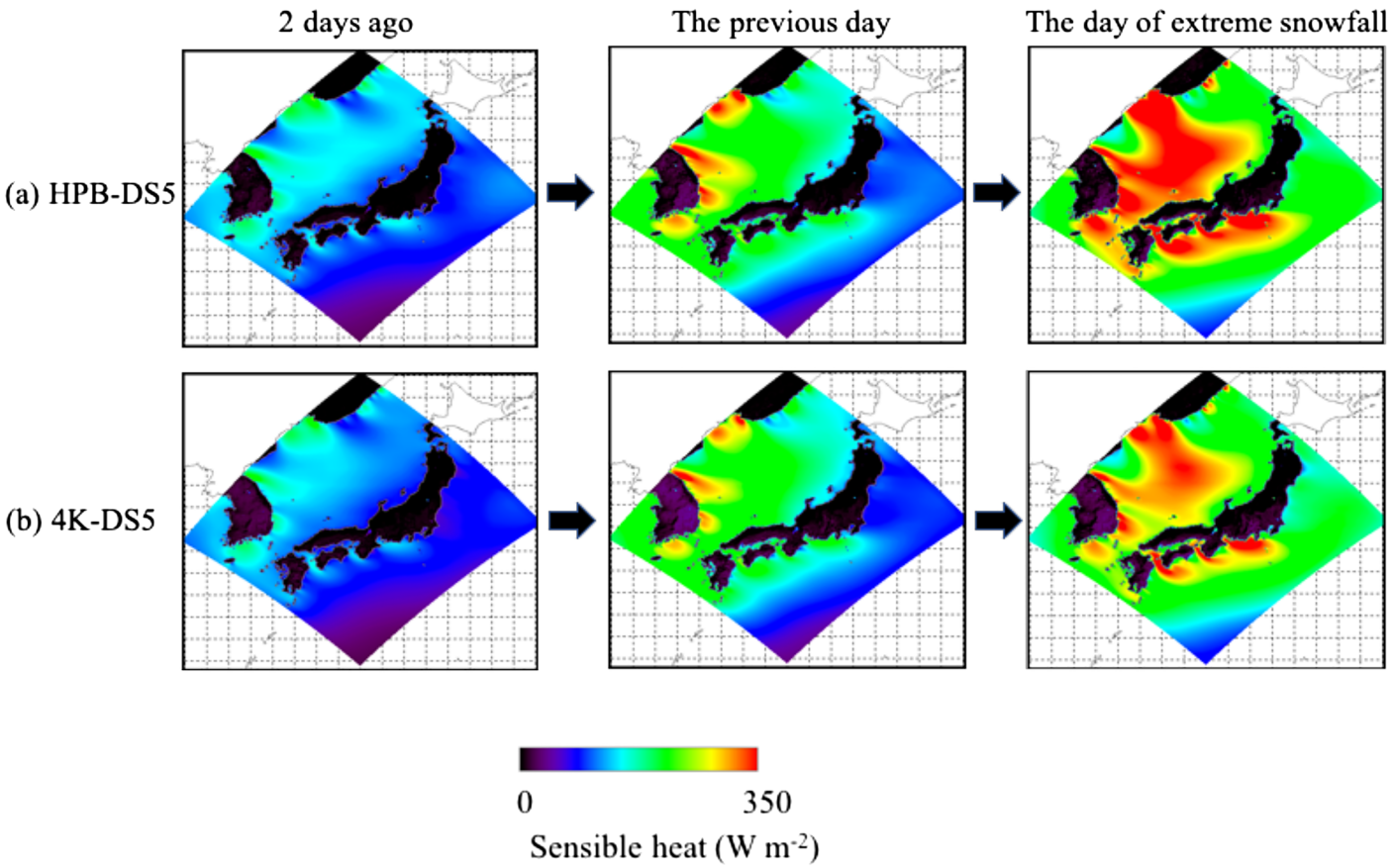

Figure 7. As in Figure 6, but for spatial variations of sensible heat flux. Sensible heat flux was directly calculated by the NHRCM.

because of the lower temperature and topographic upward flow (Figures 2b and 2c). The distribution is consistent with observations from the major Japanese observation networks: The Automated Meteorological Data Acquisition System (AMeDAS) and the Japanese 55-year reanalysis (JRA55) data set (e.g., Takahashi & Idenaga, 2013). A comparison of climatological values of accumulated snowfall between HPB-DS5 and 4K-DS5 shows decreasing trends in response to the warming shift (the average and maximum difference are 9.6 and 282.1 mm 3 month^{-1}, respectively). Most regions showed such a distribution, and a decline in average snowfall is prominent along the coast of the Sea of Japan.

Central Japan was divided into two regions according to snowfall-causing atmospheric pressure pattern, and frequency distributions of extreme snowfall were statistically analyzed using the GEV theory; a PDF of extreme events is generated from annual maximum daily snowfall. The winter monsoon pattern (the ocean effect snow pattern) region follows an extremal Weibull distribution (Figure 3a), and the shape parameter of HPB-DS5 (−0.17) is larger than that of 4K-DS5 (−0.24). Thus, future warming is projected to clearly increase the frequency of smaller extreme snowfall events. In contrast, the south coast cyclone pattern (snowstorm pattern) region follows a Fréchet distribution (Figure 3b), with small snowfall extreme increasing noticeably responsive to the warming shift. Unexpectedly large extreme snowfall may occur even in the warmer future climate. The two regions have starkly different patterns, and the frequency of extreme snowfall in the winter monsoon pattern region only slightly change for the warming shift. Thus, the impact of temperature rise on the winter monsoon pattern region may be smaller than that on the south coast cyclone pattern region.

We examined the difference in extreme snowfall between HPB-DS5 and 4K-DS5 in the winter monsoon pattern region (Figure 4). An increasing trend was found in mountainous areas and a decreasing trend was found in coastal areas (Figure 4a), consistent with previous work (e.g., Frei et al., 2018; Kawase et al., 2016; Räisänen, 2016). In addition, the PDF in each region of increasing or decreasing extreme snowfall

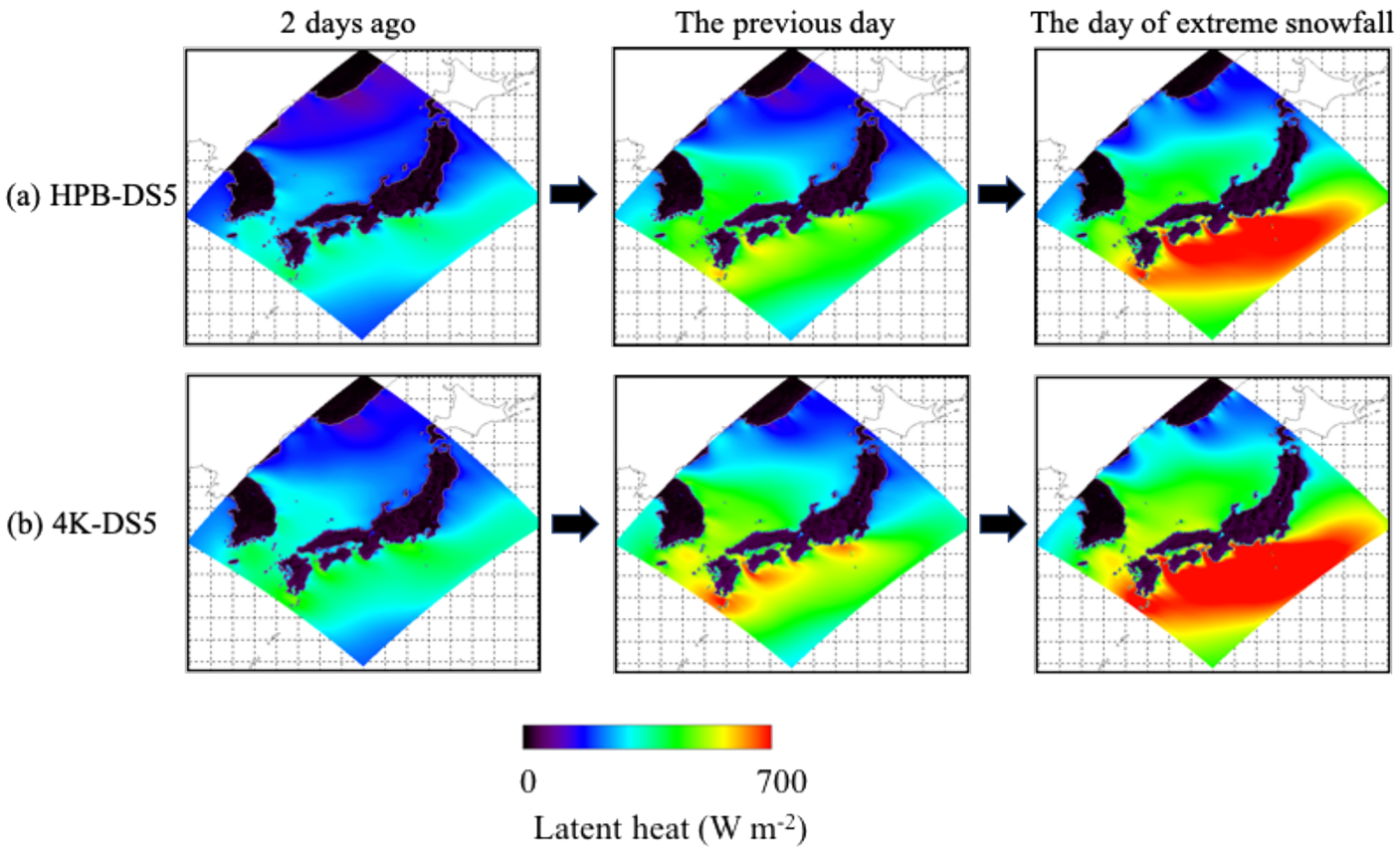

Figure 8. As in Figure 6, but for spatial variations of latent heat flux. Latent heat flux was directly calculated by the NHRCM.

in the winter monsoon pattern region showed different patterns (Figure 4b). In regions where extreme snowfall increases ("Area that is higher in 4K"), the PDF indicates that the averaged value of the extreme snowfall slightly raising up; the frequency of smaller extreme snowfall increases; and the statistical maximum value decreases (87.4 and 79.2 mm/day in HPB-DS5 and 4K-DS5, respectively). Regions with a decreasing trend in extreme snowfall ("Area that is higher in HPB") showed that an overall extreme snowfall is weakening and the frequency of large extreme snowfall decreases drastically. Previous studies have shown that extreme snowfall events decrease with global warming, except in the lowest temperature areas (de Vries et al., 2014; Frei et al., 2018; Lute et al., 2015; Räisänen, 2016). Thus, we spatially examined the threshold for water phase change (~0 °C) by composite analysis of air temperature on extreme snowfall days (Figures 5a and 5b). The spatial variations are consistency to that of extreme snowfall. The boundary line of the threshold for water phase change spatially changed toward higher altitude along with global warming, leading to clearly increase the area that is above 0 °C in coastal areas. It suggests that the temperature rise decreases the amount of precipitation that falls as snow. Thus, the spatial variations of extreme snowfall amount strongly depend on air temperature changes near the threshold of the rain-snow phase transition.

As snowfall in the winter monsoon pattern region depends on the amount of heat and water supplied from the Sea of Japan by cold air outbreaks, we examined cold air masses and latent and sensible heat fluxes for 3 days before extreme snowfall events in composite analyses (Figures 6–8). Cold air masses generally flow in plains and valleys on Eurasia toward the Japanese islands and gradually strengthen approaching the onset of extreme snowfall (Figure 6). Sensible heat follows the same spatiotemporal pattern (Figure 7). The warming shift results in an intensification of cold air outbreaks throughout the study area during extreme snowfall events. As a result, latent heat flux increases lead to an overall increase in water and heat supply from the ocean (Figure 8). The slightly decreasing sensible heat flux suggests that the temperature difference between the atmosphere and ocean is reduced by an increase in the air temperature of the cold air outbreak itself.

a) Comparison of matching extreme days between snowfall and three factors.

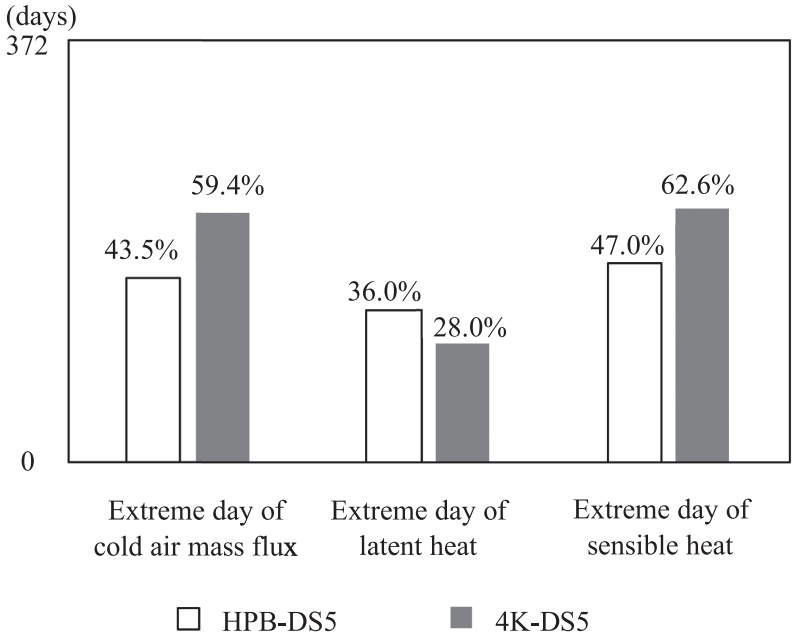

b) Domain used to calculate extreme days for the three fluxes (southern Sea of Japan).

Figure 9. (a) Percentage of matching extreme days between snowfall and cold air mass flux, latent heat flux, and sensible heat flux for HPB- and 4K-DS5. Matching extreme days indicate that an extreme snowfall event occurred 3 days after an extreme event for air mass, latent heat, or sensible heat flux. The coincidence rate (%) is the matching days divided by 372 (the number of extreme snowfall days) × 100%. (b) Area used in the calculation of the three constraining factors.

To examine the driving factor of extreme snowfall events, we extracted extreme days for three fluxes using statistical rules of the extreme value theory. These days were then compared to days of extreme snowfall (Figures 9a and 9b). The coincidence rates of the cold air mass and sensible heat fluxes increase with the warming shift (from 43.5% to 59.4% and 47.0% to 62.6%, respectively), and those of the latent heat flux decrease (from 36% to 28%). These and previous results related to increasing cold air mass and latent heat fluxes and decreasing sensible heat fluxes (Figures 6–8) indicate that cold air mass flux is the most significant constraining factor among the three parameters. The warming shift decreases the possibility that latent heat behaviors as the constraining factor and increases that of the other two parameters, because of transporting sufficient heat and water from ocean to the atmosphere possible.

4. Discussion

Here we demonstrate that snowfall decreases with the warming shift through a change in the phase of water from solid to liquid (Figure 2b). Generally, global-scale model studies have shown that future snowfall frequency and snow cover areas gradually decrease with global warming (e.g., IPCC AR5, 2013; Vaughan et al., 2013), consistent with our projections. Moreover, our spatially resolved results are consistent with point-scale observations of significant snow cover decrease due to declining snowfall and increasing snow melt

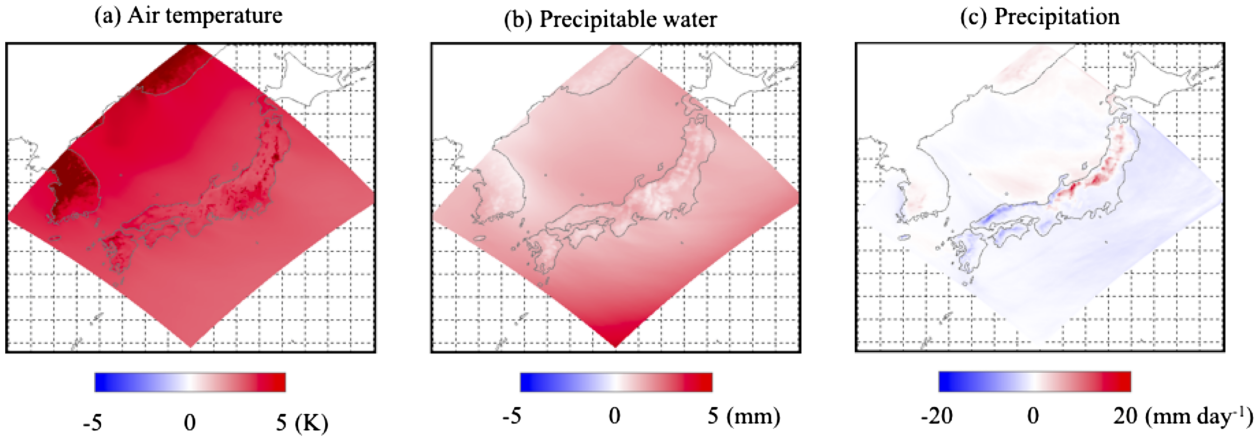

Figure 10. (a) Differences in air temperature, (b) precipitable water vapor, and (c) precipitation between HPB- and 4K-DS5 ("4K-DS5 − HPB-DS5") during extreme snowfall events in the winter monsoon pattern region.

(e.g., Collins et al., 2013; Kapnick & Delworth, 2013; Kapnick & Hall, 2012; Knowles et al., 2006; Mote et al., 2005; Stewart et al., 2005). The rate of decrease is much more pronounced in the coastal area of the Sea of Japan where there has historically been large snow accumulation. Our high-resolution ensemble simulations thus improve the scientific understanding of the regional impacts of warming.

We also find that the warming shift significantly decreases extreme snowfall in the south coast cyclone pattern region, but does not greatly affect the winter monsoon pattern region. An extreme snowfall event generally requires meteorological conditions that include both stronger precipitation and a low temperature field. These two factors are largely affected by temperature rise. For precipitation activity, a warming air parcel increases the saturated vapor pressure following the Clausius-Clapeyron relation, leading to more winter precipitation (e.g., Frei et al., 2006; Kew et al., 2011; Lenderink & van Meijgaard, 2008; O'Gorman & Schneider, 2009; Pall et al., 2006; van Haren et al., 2012). This relationship is noticeable in our simulation results as higher air temperature and more precipitable water vapor during extreme snowfall events in the winter monsoon pattern region (Figure 10). However, although the coastal plain region of the Sea of Japan is warmer, precipitation in this region decreases. Increasing saturated vapor pressure decreases the rate of water condensation, and thus more atmospheric water is retained in the gas phase. The coldest mountain region follows an increasing snowfall trend because of intensification of precipitation combined with precipitable water remaining in the solid phase despite the warming shift. In our study area, extreme snowfall events are found to change through the following three mechanisms, depending on the region: (1) the frequency of large extreme snowfall events decreases because of both effects of temperature rise and decreasing precipitation in the southern part; (2) the frequency of large extreme snowfall events decreases because of just effect of temperature rise in the plains and low-altitude areas of northern part; and (3) the frequency of larger extreme snowfall events increases because of effect of increasing precipitation in mountainous (the coldest) areas of northern part.

Here we summarize the mechanism leading to extreme snowfall in the winter monsoon pattern region under projected warming conditions, based on an existing snowfall mechanism for the Sea of Japan side of Japan (Figure 11; e.g., Magono, 1966; Takahashi et al., 2013). Approaching the onset of extreme snowfall, the cold air mass flux flowing from Siberia toward the Sea of Japan increases with the warming shift, and the temperature of the cold air parcel itself increases as its temperature difference with the sea surface decreases (Figures 6 and 7). A relatively cold air mass receives large amounts of energy and water from the ocean, and is projected to receive even larger amounts of energy and water under future warming conditions responsive to the cold dry air mass increases (Figures 7 and 8). Subsequently, the warming and wetting of low-altitude air causes a convective instability, leading to the generation and development of a snow cloud. By increasing the total heat and water supplied by the ocean, convection also tends to become unstable. These results suggest that the intensification of overall convective activity may lead to the development of more snow clouds above the unstable layer (Takahashi et al., 2013). Although clouds reaching the Japanese islands in the East Asian monsoon increase the potential for terrestrial rainfall, land precipitation does not necessarily increase

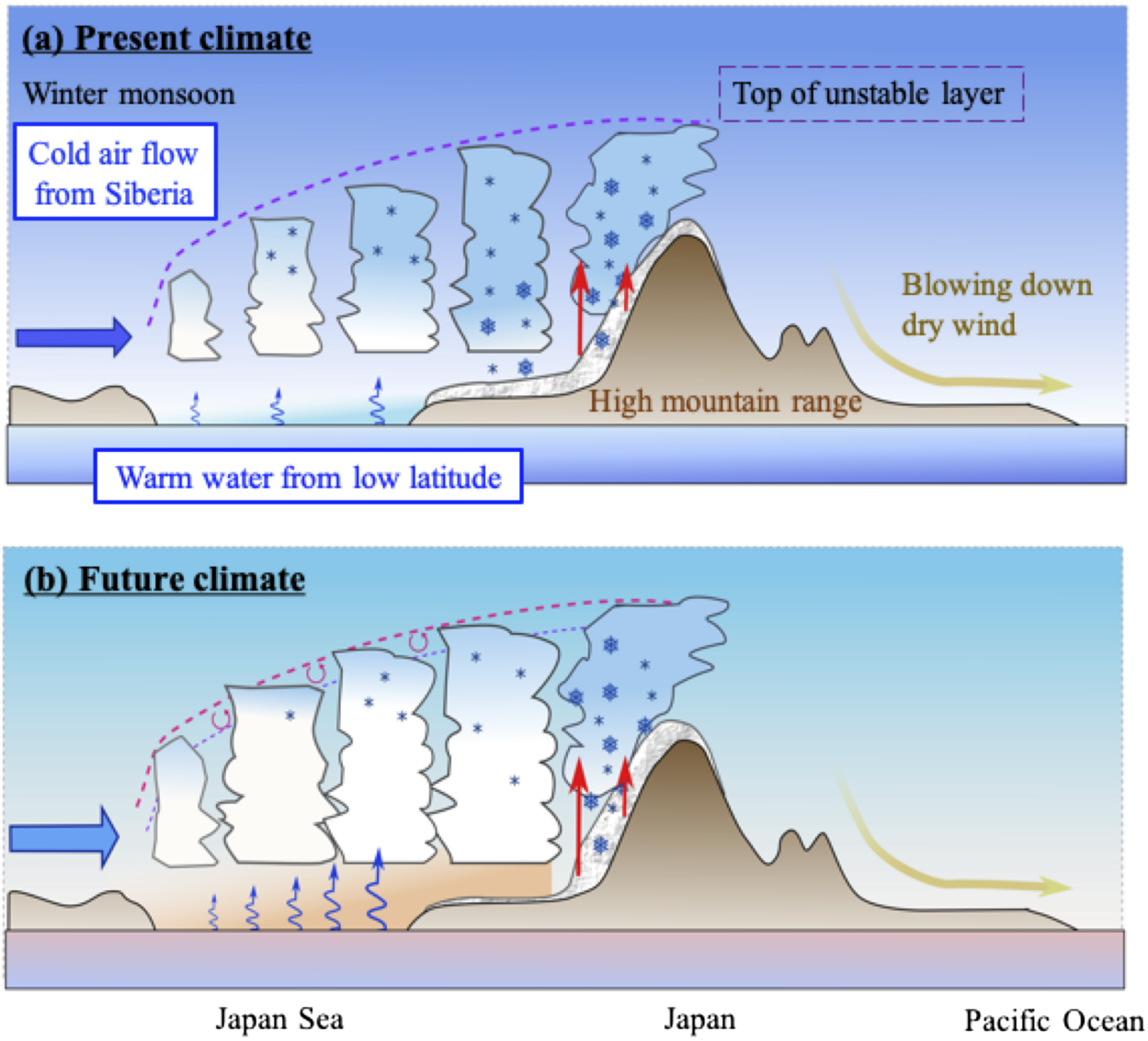

Figure 11. Mechanism leading to an extreme snowfall event in the winter monsoon pattern region over the Sea of Japan side of Japan in (a) the present and (b) future warmer climate.

over the whole winter monsoon pattern region. The reason for this may be related to orographic updraft, which facilitates precipitation by mixing supercooled water and ice crystals in snow clouds (i.e., the mountain snow pattern). In fact, the plain area along the coast of the Sea of Japan has a relatively smaller effect of the orographic updraft, and changes little and may decrease slightly in precipitation even though precipitable water increases (Figures 2b and 10). However, over the mountains, air in the lower layer is cooled by the orographic updraft, and condensing water vapor leads to increased precipitation. Therefore, future temperature increases are projected to strengthen precipitation over mountainous areas and convective activity over the Sea of Japan, leading to an enhancement in extreme snowfall events in the winter monsoon pattern region.

We conclude that the mechanism discussed above causes the difference in response of extreme snowfall to temperature rise between the Japan Sea side and the Pacific side of Japanese islands, and is expected to result in greater regional variation of extreme snowfall amounts. To understand the difference between "the plains and low-altitude areas of northern part" and "mountainous (the coldest) areas of northern part", the relationship between global-scale temperature increases and local-scale winter precipitation must be understood. Generally, cold air outbreaks determine the amount of snowfall, and the intensity of cold air mass flux

(i.e., cold air outbreaks) is projected to decrease globally as a result of global warming (e.g., Kanno et al., 2016; Park et al., 2011; Screen et al., 2015; Vavrus et al., 2006). However, our results predict a strengthening of cold air mass flux during extreme snowfall events (Figures 6a and 6b) and an increase of the coincidence rate between extreme event days (Figure 9a), suggesting that cold air outbreaks may play an increasingly important role in extreme snowfall events. In contrast, latent heat flux increases with the warming shift (Figures 8a and 8b), and the coincidence rate between extreme latent heat and snowfall days decreases (Figure 9a). This suggests that latent heat flux will play a decreasingly important role in extreme snowfall events. To forecast the occurrence of extreme snowfall events under future warmer conditions early and accurately, it is necessary to enhance the system of meteorological monitoring relevant to both cold air outbreaks and precipitation and link mesoscale observations to synoptic-scale results.

The fact that the frequency and strength of extreme snowfall events are enhanced even in the 4-K scenario is important not only for the scientific understanding of extreme snowfall but also for natural disaster preparation and climate change adaptation over the coming decades. High-resolution, large-scale ensemble experiments generally require significant research effort and computational resources, but as noted above, their results can be used to accurately estimate extreme mesoscale events. In this study, domain-averaged values are used to identify extreme meteorological events, and thus the statistical sample of extreme events from the ensemble results are mainly of the mountain snow type (Figures 3a and 3b). However, extreme snowfall amounts may decrease with the warming shift in plain regions (Figure 4a). Understanding the difference of snowfall pattern accompanying geographical characteristics between plain and mountain areas is also relevant to climate change adaptation, because plain area has larger population. Future work will focus on advancing our understanding of local-scale extreme snowfall by analyzing polar air mass convergence zones and mesobeta-scale cyclones that cause updrafts (e.g., Tsuboki & Asai, 2004).

5. Conclusions

We conducted a 5-km resolution ensemble warming projection using the 20-km resolution d4PDF data set for lateral boundary conditions and examined the change in extreme snowfall with warming, and related mechanisms by comparing results for present, near-, and far-future climate scenarios. The model experiment, computed using the Earth Simulator, provided >1,000 years of simulated climate data. To accurately assess the frequency of occurrence of these rare events, we increased the sample set using the extreme value theory (GEV distribution). We analyzed cold air outbreaks using the isentropic cold air analysis tool, and determined the mechanism of extreme snowfall events in the winter monsoon pattern and assessed the related meteorological processes.

The response to warming of extreme snowfall in winter monsoon regions is found to differ from that in south coast cyclone pattern regions. The domain-averaged amount of extreme snowfall in the south coast cyclone pattern regions is found to decrease with warming in the HPB-DS5 to 2K- and 4K-DS5 scenarios, but that in the winter monsoon pattern regions showed no significant difference among the three climate scenarios. This study mainly focused on future changes to extreme snowfall events in winter monsoon pattern regions. Results from composite analyses of the ensemble experiment reveal that future warming greatly increases saturated water vapor according to the Clausius-Clapeyron relationship, leading to an increase in winter precipitation; future warming is projected to result in a crossing of the threshold for water phase change in part of the studied region. Three regional mechanisms for snowfall are here determined: (1) The frequency of large extreme snowfall events decreases because of both effects of temperature rise and decreasing precipitation in the southern part; (2) the frequency of large extreme snowfall events decreases because of just effect of temperature rise in the plains and low-altitude areas of northern part; and (3) the frequency of larger extreme snowfall events increases because of effect of increasing precipitation in mountainous (the coldest) areas of northern part. On the Sea of Japan side, future warming is projected to lead to an increase in dry cold air mass flux from Siberia, which increases the frequency of snow cloud formation by supplying heat and water from the ocean. This suggests a need to enhance the monitoring of cold air outbreaks for extreme weather forecasting under warming conditions.

To further advance the scientific understanding of extreme snowfall events, the approach applied here of examining each meteorological process related to extreme snowfall should be applied to each region with

a similar mechanism for snowfall resulting from cold air outbreaks. The mechanisms for extreme snowfall found here will benefit the development of improved forecasts of heavy snowfall and long-term disaster preparedness. Additional analyses of specific meteorological phenomena related to local-scale snowfall will improve our understanding of the spatial distribution of extreme snowfall events. Although high-resolution, large-scale ensemble dynamical downscaling requires significant research effort and computational resources, this study demonstrates that such an investment is worth the effort given its relevance to extreme meteorological phenomena.

Acknowledgments
The corresponding author is deeply grateful to all members of Atmospheric Science Laboratory in Tohoku University and the Social Implementation Program on Climate Change Adaptation Technology (SI-CAT). Regarding the model setting of NHRCM, we received the good support from R. Ito. We are grateful to the JMA climate data set providers and the NHRCM developer team. All data and model for this paper are properly cited and referred to in the reference list. This research was mainly supported by SI-CAT of the Ministry of Education, Culture, Sports, Science and Technology (MEXT), Japan, and partly supported by the Integrated Research Program for Advancing Climate Models (TOUGOU program) from MEXT, and the Environment Research and Technology Development Fund (S-15) of the Ministry of the Environment, Japan. The large-scale ensemble simulation was operated in the Earth Simulator (ES) of JAMSTEC. The d4PDF was also produced with ES as "Strategic Project with Special Support" under corporations among the Program for Risk Information on Climate Change (SOUSEI), SI-CAT, TOUGOU, and the Data Integration and Analysis System (DIAS) from MEXT.

References

Aoyagi, T., & Seino, N. (2011). A square prism urban canopy scheme for the NHM and its evaluation on summer conditions in the Tokyo metropolitan area, Japan. *Journal of Applied Meteorology and Climatology*, *50*, 1476–1496. https://doi.org/10.1175/2011JAMC2489.1

Carril, A. F., Menéndez, C. G., Remedio, A. R. C., Robledo, F., Sörensson, A., Tencer, B., et al. (2012). Performance of a multi-RCM ensemble for South Eastern South America. *Climate Dynamics*, *39*(12), 2747–2768. https://doi.org/10.1007/s00382-012-1573-z

Christidis, N., Stott, P. A., Scaife, A. A., Arribas, A., Jones, G. S., Copsey, D., et al. (2013). A new HadGEM3-A-based system for attribution of weather- and climate-related extreme events. *Journal of Climate*, *26*, 2756–2783. https://doi.org/10.1175/JCLI-D-12-00169.1

Coles, S. (2001). *An introduction to statistical modeling of extreme values*. Springer, 208 pp. https://doi.org/10.1007/978-1-4471-3675-0

Collins, M., Knutti, R., Arblaster, J., Dufresne, J.-L., Fichefet, T., Friedlingstein, P., et al. (2013). Long-term climate change: Projections, commitments and irreversibility. In T. F. Stocker, D. Qin, G. K. Plattner, M. Tignor, S. K. Allen, J. Boschung, A. Nauels, Y. Xia, V. Bex, & P. M. Midgley (Eds.), *Climate change 2013: The physical science basis* (pp. 1029–1136). Cambridge, United Kingdom and New York, NY, USA: Cambridge University Press. https://doi.org/10.1017/CBO9781107415324

de Vries, H., Lenderink, G., & van Meijgaard, E. (2014). Future snowfall in western and central Europe projected with a high-resolution regional climate model ensemble. *Geophysical Research Letters*, *41*, 4294–4299. https://doi.org/10.1002/2014GL059724

Deser, C., Phillips, A., Bourdette, V., & Teng, H. (2012). Uncertainty in climate change projections: The role of internal variability. *Climate Dynamics*, *38*, 527–546. https://doi.org/10.1007/s00382-010-0977-x

Deushi, M., & Shibata, K. (2011). Development of a Meteorological Research Institute Chemistry—Climate model version 2 for the study of tropospheric and stratospheric chemistry. *Papers in Meteorology and Geophysics*, *62*, 1–46. https://doi.org/10.2467/mripapers.62.1

Fowler, H., Ekstrom, M., Blenkinsop, S., & Smith, A. (2007). Estimating change in extreme European precipitation using a multimodel ensemble. *Journal of Geophysical Research*, *112*, D18104. https://doi.org/10.1029/2007JD008619

Frei, C., Schöoll, R., Fukutome, S., Schmidli, J., & Vidale, P. L. (2006). Future change of precipitation extremes in Europe: Intercomparison of scenarios from regional climate models. *Journal of Geophysical Research*, *111*, D06105. https://doi.org/10.1029/2005JD005965

Frei, P., Kotlarski, S., Liniger, M. A., & Schär, C. (2018). Future snowfall in the Alps: Projections based on the EURO-CORDEX regional climate models. *The Cryosphere*, *12*, 1–24. https://doi.org/10.5194/tc-12-1-2018

Fujibe, F. (2011). Discussion of fitness analysis for selecting distribution functions in extreme value analysis. *Tenki*, *58*(9), 765–775. (in Japanese with English abstract). [available online at https://www.metsoc.jp/tenki/english/tenki_abst11.html]

Fujita, M., Mizuta, R., Ishii, M., Endo, H., Sato, T., Okada, S., et al. (2018). Precipitation changes in a climate with 2 K surface warming from large ensemble simulations by 60 km global and 20 km regional atmospheric models. *Journal of Geophysical Research: Letter*, *46*, 435–442. https://doi.org/10.1029/2018GL079885

Guan, B., Molotch, N. P., Waliser, D. E., Fetzer, E. J., & Neiman, P. J. (2013). The 2010/2011 snow season in California's Sierra Nevada: Role of atmospheric rivers and modes of large-scale variability. *Water Resources Research*, *49*, 6731–6743. https://doi.org/10.1002/wrcr.20537

Hirahara, S., Ishii, M., & Fukuda, Y. (2014). Centennial-scale sea surface temperature analysis and its uncertainty. *Journal of Climate*, *27*, 57–75. https://doi.org/10.1175/JCLI-D-12-00837.1

Hirai, M., Sakashita, T., Kitagawa, H., Tsuyuki, T., Hosaka, M., & Oh'izumi, M. (2007). Development and validation of a new land surface model for JMA's operational global model using the CEOP observation dataset. *J. Meteor. Soc. Japan*, *85A*, 1–24. https://doi.org/10.2151/jmsj.85A.1

Ikawa, M., Mizuno, H., Matsuo, T., Murakami, M., Yamada, Y., & Saito, K. (1991). Numerical modeling of the convective snow cloud over the Sea of Japan—Precipitation mechanism and sensitivity to ice crystal nucleation rates. *Journal of the Meteorological Society of Japan*, *69*, 641–667. https://doi.org/10.2151/jmsj1965.69.6_641

Inatsu, M., Sato, T., Yamada, T. J., Kuno, R., Sugimoto, S., Farukh, M. A., et al. (2015). Multi-GCM by multi-RAM experiments for dynamical downscaling on summertime climate change in Hokkaido. *Atmospheric Science Letters*, *16*, 297–304. https://doi.org/10.1002/asl2.557

IPCC AR5 (2013). Summary for policymakers. contribution of working group I to the fifth assessment report of the Intergovernmental Panel on Climate Change. In T. F. Stocker, D. Qin, G. K. Plattner, M. Tignor, S. K. Allen, J. Boschung, A. Nauels, Y. Xia, V. Bex, & P. M. Midgley (Eds.), *Climate change 2013: The physical science basis* (pp. 3–29). Cambridge, United Kingdom and New York, NY, USA: Cambridge University Press. https://doi.org/10.1017/CBO9781107415324

IPCC AR5 (2014). Contribution of working group II to the fifth assessment report of the Intergovernmental Panel on Climate Change. In C. B. Field, V. R. Barros, D. J. Dokken, K. J. Mach, M. D. Mastrandrea, T. E. Bilir, M. Chatterjee, K. L. Ebi, Y. O. Estrada, R. C. Genova, B. Girma, E. S. Kissel, A. N. Levy, S. MacCracken, P. R. Mastrandrea, & L. L. White (Eds.), *Climate change 2014: Impacts, adaptation, and vulnerability. Part A: Global and sectoral aspects* (pp. 1–1132). Cambridge, United Kingdom and New York, NY, USA: Cambridge University Press. https://doi.org/10.1017/CBO9781107415379

Ishizaki, N. N., Shiogama, H., Takahashi, K., Emori, S., Dairaku, K., Kusaka, H., et al. (2012). An attempt to estimate of probabilistic regional climate analogue in a warmer Japan. *Journal of the Meteorological Society of Japan*, *90B*, 65–74. https://doi.org/10.2151/jmsj.2012-B05

Ito, R., Aoyagi, T., Hori, N., Oh'izumi, M., Kawase, H., Dairaku, K., et al. (2018). Improvement of snow depth reproduction in Japanese urban areas by the inclusion of a snowpack scheme in the SPUC model. *Journal of the Meteorological Society of Japan*, *96*, 511–534. https://doi.org/10.2151/jmsj.2018-053

Iwasaki, T., Shoji, T., Kanno, Y., Sawada, M., Ujiie, M., & Takaya, K. (2014). Isentropic analysis of polar cold airmass streams in the Northern Hemispheric winter. *Journal of the Atmospheric Sciences*, *71*(6), 2230–2243. https://doi.org/10.1175/jas-d-13-058.1

Japan Meteorological Agency (2007). *Outline of the operational numerical weather prediction at the Japan Meteorological Agency (Appendix to WMO numerical weather prediction progress report)*. Japan Meteorological Agency. 194 pp. [available online at http://www.jma.go.jp/jma/jma-eng/jma-center/nwp/outline-nwp/index.htm].

Kain, J. S., & Fritsch, J. M. (1993). Convective parameterization for mesoscale models: The Kain-Fritsch scheme. In K. A. Emanuel, & D. J. Raymond (Eds.), *The Representation of Cumulus Convection in Numerical Models* (pp. 165–170). Boston, US: Am. Meteorol. Soc. https://doi.org/10.1007/978-1-935704-13-3

Kanno, Y., Abdillah, M. R., & Iwasaki, T. (2016). Long-term trend of cold air mass amount below a designated potential temperature in Northern and Southern Hemispheric winters using reanalysis data sets. *Journal of Geophysical Research: Atmospheres*, *121*, 10138–10152. https://doi.org/10.1002/2015JD024635

Kapnick, S., & Hall, A. (2012). Causes of recent changes in western North American snowpack. *Climate Dynamics*, *38*(9-10), 1885–1899. https://doi.org/10.1007/s00382-011-1089-y

Kapnick, S. B., & Delworth, T. L. (2013). Controls of global snow under a changed climate. *Journal of Climate*, *26*, 5537–5562. https://doi.org/10.1175/JCLI-D-12-00528.1

Kawase, H., Murata, A., Mizuta, R., Sasaki, H., Nosaka, M., Ishii, M., & Takayabu, I. (2016). Enhancement of heavy daily snowfall in central Japan due to global warming as projected by large ensemble of regional climate simulations. *Climatic Change*, *139*, 265–278. https://doi.org/10.1007/s10584-016-1781-3

Kawase, H., Sasai, T., Yamazaki, T., Ito, R., Dairaku, K., Sugimoto, S., et al. (2018). Characteristics of synoptic conditions for heavy snowfall in western to northeastern Japan analyzed by the 5-km regional climate ensemble experiments. *Journal of the Meteorological Society of Japan*, *96*(2), 161–178. https://doi.org/10.2151/jmsj.2018-022

Kawase, H., Suzuki, C., Ishizaki, N. N., Uno, F., Iida, H., & Aoki, K. (2015). Simulations of monthly variation in snowfall over complicated mountainous areas around Japan's Northern Alps. *SOLA*, *11*, 138–143. https://doi.org/10.2151/sola.2015-032

Kew, S., Selten, F., Lenderink, G., & Hazeleger, W. (2011). Robust assessment of future changes in extreme precipitation over the Rhine basin using a GCM. *Hydrology and Earth System Sciences*, *15*, 1157–1166. https://doi.org/10.5194/hess-15-1157-2011

Khaliq, M. N., Sushama, L., Monette, A., & Wheater, H. (2014). Seasonal and extreme precipitation characteristics for the watersheds of the Canadian Prairie Provinces as simulated by the NARCCAP multi-RCM ensemble. *Climate Dynamics*, *44*(1-2), 255–277. https://doi.org/10.1007/s00382-014-2235-0

Kitagawa, H. (2000). Radiation processes. *Separate Volume of the Annual Report of NPD*, *46*, 16–31. (in Japanese)

Knowles, N., Dettinger, M. D., & Cayan, D. R. (2006). Trends in snowfall versus rainfall in the western United States. *Journal of Climate*, *19*, 4545–4559. https://doi.org/10.1175/JCLI3850.1

Kobayashi, S., Ota, Y., Harada, Y., Ebita, A., Moriya, M., Onoda, H., et al. (2015). The JRA-55 Reanalysis: General specifications and basic characteristics. *Journal of the Meteorological Society of Japan*, *93*, 5–48. https://doi.org/10.2151/jmsj.2015-001

Lenderink, G., & van Meijgaard, E. (2008). Increase in hourly precipitation extremes beyond expectations from temperature. *Nature Geoscience*, *1*, 511–514. https://doi.org/10.1038/ngeo262

Lute, A. C., & Abatzoglou, J. T. (2014). Role of extreme snowfall events in interannual variability of snowfall accumulation in the western United States. *Water Resources Research*, *50*, 2874–2888. https://doi.org/10.1002/2013WR014465

Lute, A. C., Abatzoglou, J. T., & Hegewisch, K. C. (2015). Projected changes in snowfall extremes and interannual variability of snowfall in the western United States. *Water Resources Research*, *51*, 960–972. https://doi.org/10.1002/2014WR016267

Magono, C. (1966). A Study on the snowfall in the winter monsoon season in Hokkaido with special reference to low land snowfall: (Investigation of natural snow crystals 6), J. Faculty of Sci. Hokkaido University, Series 7. *Geophysics*, *2*(3), 287–308.

Mizuta, R., Murata, A., Ishii, M., Shiogama, H., Hibino, K., Mori, N., et al. (2017). Over 5,000 years of ensemble future climate simulations by 60-km global and 20-km regional atmospheric models. *Bulletin of the American Meteorological Society*, *98*, 1383–1398. https://doi.org/10.1175/BAMS-D-16-0099.1

Mote, P. W., Hamlet, A. F., Clark, M. P., & Lettenmaier, D. P. (2005). Declining mountain snowpack in western North America. *Bulletin of the American Meteorological Society*, *86*, 39–49. https://doi.org/10.1175/BAMS-86-1-39

Murata, A., Sasaki, H., Hanafusa, M., & Kurihara, K. (2013). Estimation of urban heat island intensity using biases in surface air temperature simulated by a nonhydrostatic regional climate model. *Theoretical and Applied Climatology*, *112*, 351–361. https://doi.org/10.1007/s00704-012-0739-2

Nakanishi, M., & Niino, H. (2004). An improved Mellor-Yamada level-3 model: Its design and verification. *Boundary-Layer Meteorology*, *112*, 1–31. https://doi.org/10.1023/b:boun.0000020164.04146.98

O'Gorman, P. A. (2014). Contrasting responses of mean and extreme snowfall to climate change. *Nature*, *512*, 416–418. https://doi.org/10.1038/nature13625

O'Gorman, P. A., & Schneider, T. (2009). The physical basis for increases in precipitation extremes in simulations of 21st century climate change. *PNAS*, *106*, 14773–14777. https://doi.org/10.1073/pnas.0907610106

Pall, P., Allen, M. R., & Stone, D. A. (2006). Testing the Clausius–Clapeyron constraint on changes in extreme precipitation under CO_2 warming. *Climate Dynamics*, *28*, 351–363. https://doi.org/10.1007/s00382-006-0180-2

Park, T. W., Ho, C. H., Jeong, S. J., Choi, Y. S., Park, S. K., & Song, C. K. (2011). Different characteristics of cold day and cold surge frequency over east Asia in a global warming situation. *Journal of Geophysical Research-Atmospheres*, *116*, D12118. https://doi.org/10.1029/2010JD015369

Räisänen, J. (2016). Twenty-first century changes in snowfall climate in Northern Europe in ENSEMBLES regional climate models. *Climate Dynamics*, *46*, 339–353. https://doi.org/10.1007/s00382-015-2587-0

Sasaki, H., Murata, A., Hanafusa, M., Oh'izumi, M., & Kurihara, K. (2011). Reproducibility of present climate in a non-hydrostatic regional climate model nested within an atmosphere general circulation model. *SOLA*, *7*, 173–176. https://doi.org/10.2151/sola.2011-044

Sato, N., Sellers, P. J., Randall, D. A., Schneider, E. K., Shukla, J., Kinter, J. L. III, et al. (1989). Effect of implementing the simple biosphere model in a general circulation model. *Journal of the Atmospheric Sciences*, *46*, 2757–2782. https://doi.org/10.1175/1520-0469(1989)046<2757:eoitsb>2.0.co;2

Screen, J. A., Deser, C., & Sun, L. (2015). Reduced risk of north American cold extremes due to continued Arctic sea ice loss. *Bulletin of the American Meteorological Society*, *96*, 1489–1503. https://doi.org/10.1175/BAMS-D-14-00185.1

Sellers, P. J., Mintz, Y., Sud, Y. C., & Dalcher, A. (1986). A Simple Biosphere model (SiB) for use within general circulation models. *Journal of the Atmospheric Sciences*, *43*, 505–531. https://doi.org/10.1175/1520-0469(1986)043<0505:ASBMFU>2.0.CO;2

Shoji, T., Kanno, Y., Iwasaki, T., & Takaya, K. (2014). An isentropic analysis of the temporal evolution of East Asian cold air outbreaks. *Journal of Climate*, *27*(24), 9337–9348. https://doi.org/10.1175/JCLI-D-14-00307.1

Sommeria, G., & Deardorff, J. W. (1977). Subgrid-Scale Condensation in Models of Nonprecipitating Clouds. *Journal of the Atmospheric Sciences*, *34*, 344–355. https://doi.org/10.1175/1520-0469(1977)034<0344:SSCIMO>2.0.CO;2

Stewart, I. T., Cayan, D. R., & Dettinger, M. D. (2005). Changes toward earlier streamflow timing across Western North America. *Journal of Climate*, *18*, 1136–1155. https://doi.org/10.1175/JCLI3321.1

Sugimoto, S., Ito, R., Dairaku, K., Kawase, H., Sasaki, H., Watanabe, S., et al. (2018). Impact of spatial resolution on simulated consecutive dry days and near-surface temperature over the central mountains in Japan. *SOLA*, *14*, 46–51. https://doi.org/10.2151/sola.2018-008

Takahashi, H. G., & Idenaga, T. (2013). Impact of SST on precipitation and snowfall on the Sea of Japan side in the winter monsoon season: Timescale dependency. *Journal of the Meteorological Society of Japan*, *91*, 639–653. https://doi.org/10.2151/jmsj.2013-506

Takahashi, H. G., Ishizaki, N. N., Kawase, H., Hara, M., Yoshikane, T., Ma, X., & Kimura, F. (2013). Potential impact of sea surface temperature on winter precipitation over the Japan Sea side of Japan: A regional climate modeling study. *Journal of the Meteorological Society of Japan*, *91*, 471–488. https://doi.org/10.2151/jmsj.2013-404

Tsuboki, K., & Asai, T. (2004). The multi-scale structure and development mechanism of mesoscale cyclones over the sea of Japan in winter. *Journal of the Meteorological Society of Japan*, *82*, 597–621. https://doi.org/10.2151/jmsj.2004.597

van Haren, R., van Oldenborgh, G. J., Lenderink, G., Collins, M., & Hazeleger, W. (2012). SST and circulation trend biases cause an underestimation of European precipitation trends. *Climate Dynamics*, *40*, 1–20. https://doi.org/10.1007/s00382-012-1401-5

Vaughan, D. G., Comiso, J. C., Allison, I., Carrasco, J., Kaser, G., Kwok, R., et al. (2013). Observations: Cryosphere. In T. F. Stocker, D. Qin, G. K. Plattner, M. Tignor, S. K. Allen, J. Boschung, A. Nauels, Y. Xia, V. Bex, & P. M. Midgley (Eds.), *Climate change 2013: The physical science basis* (Chap. 4, pp. 317–382). Cambridge, United Kingdom and New York, NY, USA: Cambridge University Press. 317-382, https://doi.org/10.1017/CBO9781107415324

Vavrus, S., Walsh, J. E., Chapman, W. L., & Portis, D. (2006). The behavior of extreme cold air outbreaks under greenhouse warming. *International Journal of Climatology*, *26*, 1133–1147. https://doi.org/10.1002/joc.1301

Xie, S.-P., Deser, C., Vecchi, G. A., Collins, M., Delworth, T. L., Hall, A., et al. (2015). Towards predictive understanding of regional climate change. *Nature Climate Change*, *5*, 921–930. https://doi.org/10.1038/nclimate2689

Yabu, S., Murai, S., & Kitagawa, H. (2005). Clear sky radiation scheme. *Separate Volume of the Annual Report of NPD*, *51*, 53–64. (In Japanese)

Yukimoto, S., Adachi, Y., Hosaka, M., Sakami, T., Yoshimura, H., Hirabara, M., et al. (2012). A new global climate model of the Meteorological Research Institute: MRI-CGCM3-Model description and basic performance. *Journal of the Meteorological Society of Japan*, *90A*, 23–64. https://doi.org/10.2151/jmsj.2012-A02